Korean J. Chem. Eng., 36(12), 1991-1999 (2019)
DOI: 10.1007/s11814-019-0410-z

pISSN: 0256-1115
eISSN: 1975-7220

Precursor and dispersion effects of active species on the activity of Mn-Ce-Ti catalysts for NO abatement

Xiaobo Wang*,,†, Jie Zhou*, Caojian Jiang*, Jia Wang***,†, Keting Gui****, and Hywel Rhys Thomas****

*School of Environmental Science, Nanjing Xiaozhuang University, Nanjing 211171, Jiangsu, China
**Geoenvironmental Research Centre, School of Engineering, Cardiff University, Cardiff, CF24 3AA, UK
***College of Chemical Engineering, Nanjing Forestry University, Nanjing 210037, Jiangsu, China
****School of Energy and Environment, Southeast University, Nanjing 210096, Jiangsu, China
(*Received 14 July 2019 • accepted 15 October 2019*)

Abstract−Mn-Ce-Ti catalysts were prepared by different precursors (including manganese nitrate, manganese acetate, and manganese chloride) and used for selective catalytic reduction (SCR) of NO with ammonia. The relationships among the structure, physicochemical properties, and catalytic activity were explored by N_2 adsorption/desorption, X-ray diffraction (XRD), H_2-temperature programmed reduction (H_2-TPR), NH_3-temperature programmed desorption (NH_3-TPD), X-ray photoelectron spectroscopy (XPS), high-resolution transmission electron microscopy (HR-TEM), scanning electron microprobe (SEM) and energy dispersive spectroscopy (EDS) techniques. The results show that the different Mn precursors play important roles in the catalytic activity. The Mn-Ce-Ti(N) catalyst synthesized by manganese nitrate precursor exhibits the best catalytic activity, while the Mn-Ce-Ti(C) and Mn-Ce-Ti(Cl) catalyst prepared by manganese acetate and manganese chloride, respectively, exhibit relatively low catalytic activity. The manganese nitrate precursor could promote the specific surface area and redox ability, enhance the amounts of Brønsted and Lewis acid sites, and enrich the surface active species such as Mn^{4+}, Ce^{3+} and surface chemisorbed oxygen of the catalyst, all of which will contribute to the SCR performance. Moreover, the Mn-Ce-Ti(N) catalyst possesses highly dispersed and uniform surface active species, which will result in the optimal physicochemical properties and superior catalytic performance.

Keywords: Precursor Effect, Active Species, Dispersion, NH_3-SCR, NO Abatement

INTRODUCTION

Nitrogen oxides (NO_x) emitted from the combustion process of stationary sources have posed a severe threat to the environment and human health. Several methods have been used for NO removal, and the SCR technology for NO abatement has proved to be the most effective process [1]. Currently, the widely used catalyst for SCR process is V_2O_5-WO_3(MoO_3)/TiO_2, which could yield high catalytic activity in 300-400 °C [2]. However, it also has some inherent drawbacks, such as a narrow active temperature window and toxicity of V_2O_5 [3]. Therefore, it is of great importance to develop a new catalyst that is highly active, non-VO_x species and environmentally friendly.

Based on this view, in recent years some transition metal oxides containing catalysts (including Fe, Ce, Mn, and Cu) have been widely designed and developed as SCR catalysts [1,3-10]. Among these, Mn-based catalysts have attracted much attention of researchers due to their high catalytic performance [11-14]. It is well known that manganese oxides exist as many oxidation states of Mn (Mn^{2+}, Mn^{3+}, and Mn^{4+}) and contain multiple types of labile oxygen [15]. These features are greatly influenced by several factors, such as the support, precursors, synthetic strategy, additive, and precipitant, and therefore lead to different catalytic performance. For example, Hwang synthesized MnO_x/TiO_2 catalysts by sol-gel strategy using manganese (II) nitrate, manganese (II) acetate, and manganese (III) acetate, respectively. And reported that the catalyst prepared by manganese (III) acetate yielded the highest SCR activity, which was due to the strong acid sites and high concentration of Mn^{4+} species (MnO_2) on the catalyst surface [16]. Fang et al. prepared MnO_x/TiO_2 catalysts by impregnation method using manganese (II) nitrate and manganese (II) acetate and found that the catalysts prepared by manganese (II) acetate yielded better catalytic performance, which was attributed to the proper Mn_2O_3 and Mn_3O_4 on the catalyst surface [15]. However, Peña et al. supported manganese nitrate and manganese acetate on Hombikat TiO_2 to prepare Mn/Hombikat-TiO_2 catalysts and reported the catalyst synthesized by manganese nitrate could generate a higher concentration of MnO_2 and thus exhibited better catalytic performance than that of the catalysts prepared from manganese acetate [17]. And Xu et al. loaded manganese nitrate, manganese acetate, and manganese chloride on H/beta to get Mn/beta catalysts, respectively, and found the catalysts prepared by manganese acetate exhibited the highest catalytic performance, and the superior activity was due to the enrichment of MnO_x (Mn_2O_3 and MnO_2) species, a certain amount of weak acid sites and high content of surface oxygen group [18]. Based on the description above, it can be clearly seen that precursor effect has a close relationship with the catalytic activity of the catalyst and different Mn precursor could generate different physical and chemical prop-

†To whom correspondence should be addressed.
E-mail: xb_wang88@126.com, wangjia_njfu@163.com

erties of catalysts and thus would display different catalytic activity. Such a precursor effect will be more obvious when the catalysts are synthesized by different precursors and supports as well as different preparation methods. In addition, CeO_2 is widely used as an additive to promote the catalytic performance of catalyst due to its redox properties and oxygen storage. But until now, the effect of Mn precursors on the catalytic performance of Mn-Ce-Ti catalysts has not been systemically studied. In particular, the relationship between structure and catalytic activity affected by Mn precursors is lacking report from the perspective of the textural and surface characteristics.

Therefore, in this present work, Mn-Ce-Ti catalysts were synthesized by different Mn precursors including manganese nitrate ($Mn(NO_3)_2$, 50% solution), manganese acetate ($MnC_4H_6O_4{\cdot}4H_2O$), and manganese chloride ($MnCl_2{\cdot}4H_2O$) using co-precipitation and applied to SCR reaction. The effect of Mn precursors on catalytic performance was evaluated and the relationship between structure and catalytic activity was revealed through several characterization methods from the aspect of the textural and surface characteristics.

EXPERIMENTAL

1. The Catalysts Preparation

Mn-Ce-Ti catalysts were synthesized by co-precipitation method. The specific steps are as follows: 25 g TiO_2 were added into the 150 mL deionized water with a continuous string, and then 4.36 mL $Mn(NO_3)_2$ (50% solution) and 2.17 g $Ce(NO_3)_3{\cdot}6H_2O$ were mixed in the solution until dissolved completely. Later, the ammonia solution (25 wt%) was used as precipitant until the pH reached 9-10. Then, stirred for 3 hr, aged for 48 hr at room temperature, dried at 150 °C for 6 hr in the oven, calcined at 450 °C for 5 hr after grinding. Finally, the sample was tableted, crushed and sieved to 30-60 mesh for measurement. For convenience, the sample was labeled as Mn-Ce-Ti (x) and x represented the molar ratio of Mn: Ce. With respect to the synthesis of Mn-Ce-Ti catalysts based on different Mn precursors, the synthetic strategy was the same as the description above with the fixed molar ratio of Mn : Ce=3.75. The catalysts prepared by manganese nitrate ($Mn(NO_3)_2$, 50% solution), manganese acetate ($MnC_4H_6O_4{\cdot}4H_2O$), and manganese chloride ($MnCl_2{\cdot}4H_2O$) were denoted as Mn-Ce-Ti(N), Mn-Ce-Ti(C), and Mn-Ce-Ti(Cl), respectively.

2. The Catalyst Characterization

N_2 adsorption-desorption isotherms were carried out at −196 °C on a Quantachrome Quadrisorb SI instrument. The specific surface area was obtained by the Brunauer-Emmett-Teller (BET) method, and the pore volumes and pore size distribution were calculated by the Barrett-Joyner-Halenda (BJH) method. X-ray diffraction (XRD) patterns were obtained on an X-ray diffractometer (Smartlab 9, Japan) with CuKα radiation in the 2θ range between 10 and 90° to study the crystal structure of the sample. H_2 temperature-programmed reduction (H_2-TPR) experiments were executed on a chemisorption instrument (Micromeritics Autochem 2920 II) to investigate the redox properties of catalysts. About 110 mg sample was pretreated in N_2 at 200 °C for 1 hr before the reduction and then cooled to 100 °C. After that, the reduction was recorded in 10% H_2/Ar (50 mL/min) from 100 to 800 °C with a flowing rate of 10 °C/min. Temperature-programmed desorption of NH_3 (NH_3-TPD) was carried out on a chemisorption instrument (Micromeritics Autochem 2920 II) to studied the acidity of catalysts. 150 mg sample was pretreated in He at 450 °C for 1 hr. Then cooled to 100 °C, saturated with 10% NH_3/He (30 mL/min) for 1 hr, and purged with Ar for 1 hr. After that, NH_3-TPD data was recorded from 100 to 600 °C at a heating rate of 10 °C/min. X-ray photoelectron spectra (XPS) was carried out on Thermo Fisher Scientific XPS (EXCALAB 250Xi) spectroscopy with Al Kα X-ray source to study the surface elements and chemical states of the samples. The binding energies were calibrated with reference to the C 1s BE value of 284.6 eV.

Transmission electron microscopy (TEM) and high-resolution transmission electron microscopy (HR-TEM) were used to obtain the microscopic structure and crystal planes of sample on a JEOL JEM-2100 electron microscope operated at 200 kv.

Energy dispersive spectroscopy (EDS) mapping was taken on a field emission-scanning electron microscopy (FESEM, Hitachi S-4200) equipped with an energy dispersive spectrometer to obtain the dispersion of the Mn and Ce on the samples.

3. Catalytic Activity Evaluation

The SCR catalytic activity was tested in a fixed-bed reactor using a 5 mL sample (30-60 mesh). The composition of the simulated flue gas was 500 ppm NH_3, 500 ppm NO, 3% O_2, 50 ppm SO_2 (when used), 5% H_2O (when used) and balance N_2. The total gas flow rate was 1.5 L/min. All the data were recorded by a flue gas analyzer (rbr ECOM-J2KN, Germany). The NO_x conversion was calculated by the following equation:

$$\text{NO conversion} = \frac{[NO]_{inlet} - [NO]_{outlet}}{[NO]_{inlet}} \times 100 \quad (1)$$

RESULTS AND DISCUSSION

1. Catalytic Performance

To optimize the Mn loading, the effect of Mn loading on NO conversion was investigated and the results are shown in Fig. 1. For the Mn-Ce-Ti(3.125) catalyst, it exhibits the lowest catalytic activity and only 36% NO conversion can be obtained at 120 °C. With the increase of temperature, the catalytic performance is enhanced and 94% NO conversion is displayed at 240 °C. When the molar

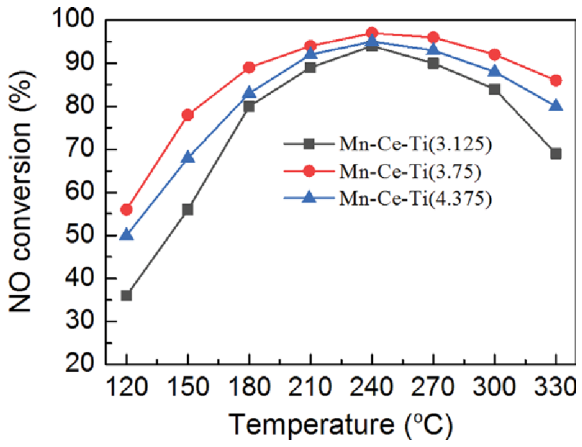

Fig. 1. Effect of Mn loading on NO conversion.

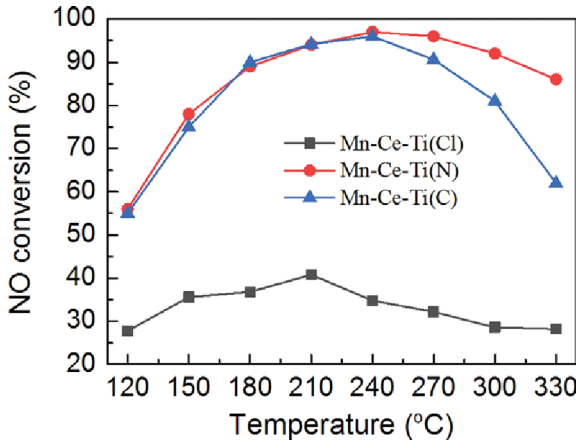

Fig. 2. Effect of Mn precursors on NO conversion.

ratio of Mn : Ce is increased to 3.75, the NO conversion of Mn-Ce-Ti(3.75) catalyst is greatly improved and more than 92% NO conversion could be yielded in a wide temperature of 210-300 °C. Further increase the molar ratio of Mn : Ce, the catalytic activity of catalyst shows some decrease. On the whole, the catalytic performance of the three catalysts is ranked by Mn-Ce-Ti(3.75)>Mn-Ce-Ti(3.125)>Mn-Ce-Ti(4.375), which demonstrates that the optimal molar ratio of Mn: Ce is 3.75.

On the basis of the optimal molar ratio of Mn and Ce, the effect of Mn precursors on the NO conversion was studied and the results are displayed in Fig. 2. It can be clearly seen that the Mn-Ce-Ti(Cl) catalyst exhibits the poorest catalytic performance and the highest catalytic activity is only 40.8% at 210 °C. For the Mn-Ce-Ti(C) catalyst, the catalytic performance is equivalent to that of Mn-Ce-Ti(N) catalyst in the low-temperature range below 240 °C. However, the catalytic activity is relatively low in the high-temperature range (>240 °C). These results definitely demonstrate that Mn-Ce-Ti(N) catalyst yields the highest catalytic activity and Mn precursors significantly influence the catalytic performance of the catalyst. Moreover, the Mn-Ce-Ti(N) catalyst exhibits the best N_2 selectivity among the three studied catalysts and excellent stability of its catalytic activity as shown in Fig. S1 and S2, respectively. And, it is well accepted that the gas hourly space velocity (GHSV) is an important parameter for the catalytic activity. The effect of GHSV on the catalytic activity of the optimum Mn-Ce-Ti(N) catalyst was investigated and the results are listed in Fig. S3, which demonstrates that the Mn-Ce-Ti(N) catalyst possesses high adaptability of the GHSV for the NO abatement. These results indicate that Mn-Ce-Ti(N) catalyst may be a promising catalyst for industrial application.

It is well known that the catalytic activity is closely related with the physical and chemical properties of catalyst such as surface area, redox ability, dispersion of active species, surface oxygen and surface acid sites in the catalytic reaction system, and many researchers have reported the relationship between the catalytic activity and the physicochemical properties of catalysts in different catalytic reactions [19-22]. For example, Lykaki et al. synthesized CeO_2 using different methods and found that the CeO_2 nanoparticles with rod-like morphology synthesized by hydrothermal method could generate excellent catalytic activity for CO oxidation, which was due to the enhanced reducibility and high content of surface oxygen species [19]. Chen et al. prepared Ce-M (M=Cu, Ni and Co) mixed oxides and used for catalytic oxidation of ethyl acetate, and reported that the catalytic activity of catalysts had a close relationship with the surface area, reducibility, calcination temperature and Ce content [20]. Li et al. reported that the catalytic activity of Mn-Ce/TiO_2-NS catalyst could be promoted by the TiO_2 {0 0 1} facets in the NH_3-SCR of NO system due to the enhancement of specific surface area and surface oxygen [22]. To gain an insight into the promotion mechanism of the Mn precursor effect, the relationship among the structure, component and the catalytic performance of catalysts prepared with different precursors will be revealed by many characterization methods and discussed below.

In addition, the effect of H_2O and SO_2 is crucial for the catalytic activity of the catalysts; many types of research have studied the effect of H_2O and SO_2 on the NO conversion of the catalysts and revealed the deactivation mechanism of the catalysts caused by them [10,23-25]. For example, Xu et al. investigated the SO_2 poisoning on the CeO_2-WO_3/TiO_2 and V_2O_5-WO_3/TiO_2 catalysts and found the formation of NH_4HSO_4 was the main reason for the deactivation of V_2O_5-WO_3/TiO_2 catalyst, while the deactivation of CeO_2-WO_3/TiO_2 was due to the production of NH_4HSO_4 as well as the Ce sulfate species [24]. France et al. studied the effect of H_2O on the catalytic activity of $FeMnO_x$ catalyst and reported that H_2O greatly reduced the NO conversion at 120 °C and displayed recovery characteristics after cutting off H_2O [10]. Therefore, we also examined the effect of H_2O and SO_2 on the catalytic activity of the optimum Mn-Ce-Ti(N) catalysts, and the results are shown in Fig. S4. It can be clearly seen that the NO conversion of the Mn-Ce-Ti(N) catalyst basically shows no obvious changes at 240 °C when H_2O is introduced into the reaction gases. The catalytic activity is quickly restored to its original level after cutting off the H_2O. When SO_2 is simultaneously added, the NO conversion exhibits a slight decrease but remains a high level of catalytic activity. After stopping the introduction of H_2O and SO_2, the catalytic activity is gradually recovered but cannot be restored to its original level completely.

2. BET Analysis

The BET surface area, pore volume and average pore diameter of different catalysts are listed in Table 1. The specific surface area for Mn-Ce-Ti(N), Mn-Ce-Ti(C) and Mn-Ce-Ti(Cl) catalysts is 22.99, 20.51 and 19.61 m^2/g, respectively, suggesting the Mn-Ce-Ti(N) catalyst prepared by manganese nitrate possesses the highest specific surface area. In addition, the pore volume and average pore diameter of the Mn-Ce-Ti(N) catalysts are also the largest among the three catalysts. It is well known that the SCR reaction is

Table 1. BET surface area and pore structure results of different catalysts

Catalysts	S_{BET} (m^2/g)	Pore volume (mm^3/g)	Average pore diameter (nm)
Mn-Ce-Ti(N)	22.99	0.056	10.05
Mn-Ce-Ti(C)	20.51	0.049	10.00
Mn-Ce-Ti(Cl)	19.61	0.043	9.13

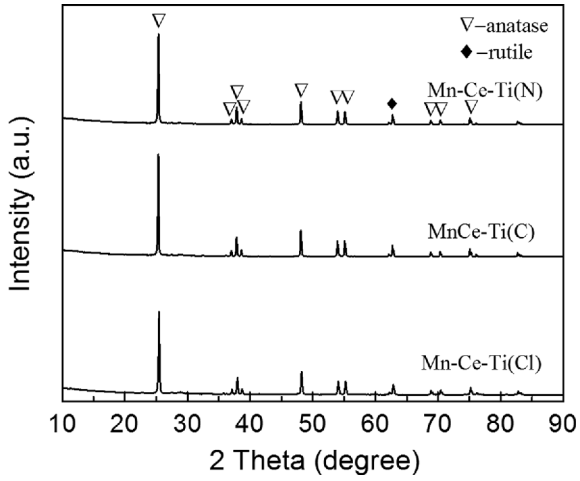

Fig. 3. XRD patterns of different catalysts.

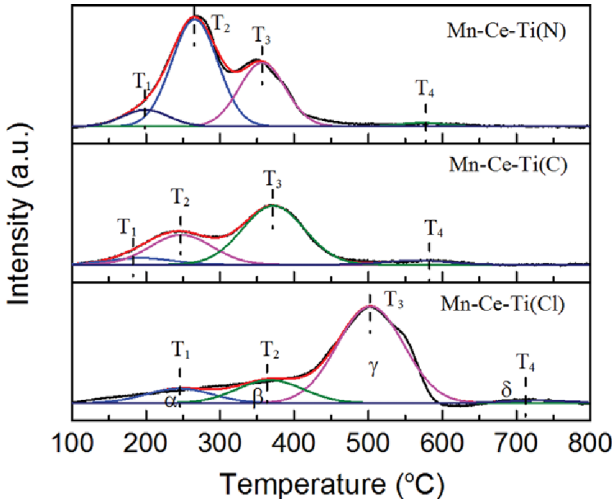

Fig. 4. H_2-TPR profiles of different catalysts.

closely related to the adsorption of reactant molecules and desorption of products. The larger specific surface area and pore volume will be beneficial to these physical mass transfer process during the reaction and therefore directly contribute to the SCR catalytic performance, which is confirmed by the experimental results of catalytic activity tests.

3. XRD Analysis

The XRD patterns of the three catalysts are displayed in Fig. 3. Strong diffraction peaks attributed to the TiO_2 anatase phase as well as a little rutile phase can be observed for all the three catalysts, while no visible phases of manganese and cerium metal oxides are detected. These results indicate that the manganese and cerium metal oxides are highly dispersed on the catalyst support, and they exist as the amorphous phases or poor crystalline states [11]. The highly dispersed active species will lead to a larger specific surface area and therefore contribute to the SCR performance. Moreover, manganese oxides displayed as the poor crystalline structure are expected to enhance the existence of surface oxygen vacancies and promote catalytic performance.

In addition, the crystallite size of the catalyst could be obtained by the Scherrer equation and the average crystallite size was calculated to be 51.8, 52.4 and 48.7 nm, respectively, from the most intensive anatase (101) diffraction peak (2θ=25.28°) of the Mn-Ce-Ti(N), Mn-Ce-Ti(C) and Mn-Ce-Ti(Cl) catalysts. The more active Mn-Ce-Ti(N) and Mn-Ce-Ti(C) catalysts possess relative bigger crystallite size, while the less active Mn-Ce-Ti(Cl) catalyst holds the smallest crystallite size. The results indicate that the average crystallite size of the anatase TiO_2 is not a key factor for the catalytic activity of the catalyst.

4. H_2-TPR Analysis

The H_2-TPR experiments were executed to investigate the redox properties of different catalysts and the corresponding results are displayed in Fig. 4 and Table 2. The H_2-TPR profiles of the three catalysts all can be divided into four peaks labeled as α, β, γ, and δ, respectively, indicating the different reduction processes of manganese and cerium metal oxides. For the H_2-TPR profile of Mn-Ce-Ti(Cl) catalyst, the two peaks at 245, and 367 °C are assigned to the reduction process of MnO_2 to Mn_2O_3 and Mn_2O_3 to Mn_3O_4, respectively [3,4]. The reduction peak at 503 °C is ascribed to the reduction steps of Mn_3O_4 to MnO, overlapping with the reduction of surface CeO_2 [10,11,26,27]. With respect to the high-temperature reduction peak located at 729 °C, it is attributed to the reduction of bulk CeO_2 [27,28]. Compared with that of Mn-Ce-Ti(Cl) catalyst, the corresponding reduction peaks for Mn-Ce-Ti(N) and Mn-Ce-Ti(C) catalysts are shifted to lower temperature (listed in Table 2), indicating that Mn precursors have a great effect on the redox ability and the redox ability of these two catalysts are significantly enhanced. This phenomenon can be caused by many factors, such as excellent dispersity, enhanced oxygen mobility and the increased active species [26,27]. Based on the results of TEM displayed in Fig. 7, the dispersity of surface active species over these three catalysts is ranked by Mn-Ce-Ti(N)>Mn-Ce-Ti(C) Mn-Ce-Ti(Cl) catalyst. The higher dispersity of surface active species will promote more active species accumulated on the catalyst surface, which will contribute to the redox ability, while the dispersity of surface active species is definitely affected by Mn precursors. Therefore, it is because of the superior dispersity of surface active species

Table 2. H_2-TPR data of different catalysts

Sample	Peak area (a.u.)				Peak temperature (°C)			
	α	β	γ	δ	T_1	T_2	T_3	T_4
Mn-Ce-Ti(N)	0.15	0.96	0.57	0.03	199	266	357	573
Mn-Ce-Ti(C)	0.08	0.37	0.72	0.05	193	248	372	565
Mn-Ce-Ti(Cl)	0.19	0.30	1.26	0.04	245	367	503	729

on Mn-Ce-Ti(N) catalyst prepared by manganese nitrate that it can exhibit excellent redox ability. Moreover, the peak area for H_2 consumption at low temperature (below 400 °C) is calculated to be 1.68, 1.17, and 0.49 for Mn-Ce-Ti(N), Mn-Ce-Ti(C), and Mn-Ce-Ti(Cl) catalyst, respectively, suggesting more reducible Mn and Ce species are accumulated on Mn-Ce-Ti(N) catalyst surface, which is confirmed by the XPS results. The redox ability can also be promoted by the larger specific surface area and thereby contribute to the SCR performance [27]. In summary, different Mn precursors will result in different specific surface area and dispersity of surface active species and thus generate different redox ability. The Mn-Ce-Ti(N) catalyst possesses the largest specific surface area, and the promoted dispersion of surface active species on the catalyst surface, and thus exhibits the best redox ability.

5. NH_3-TPD Analysis

The surface acid sites of a catalyst are crucial for the chemisorption and activation of ammonia molecules in SCR reaction. Therefore, the surface acidity of catalysts was evaluated by NH_3-TPD measurements and the results are shown in Fig. 5. As displayed in Fig. 5, all the NH_3-TPD profiles of the three catalysts prepared by different Mn precursors contain two ammonia desorption peaks located at about 142 and 518 °C, respectively. The peak I is attributed to the NH_3 desorption originating from the weak and medium acid sites, while the peak II can be ascribed to the NH_3 desorption of strong acid sites [29]. For an intuitive comparison, the peak areas of the NH_3 desorption for the three catalysts were calculated and the corresponding data are listed in Table 3. The total ammonia desorption is ranked by Mn-Ce-Ti(N)>Mn-Ce-Ti(Cl)>Mn-Ce-Ti(C) catalyst. And they show a significant difference in the amount of the NH_3 adsorbed on different acid sites. It is reported that the low-temperature desorption peaks are originated from the NH_3 desorption adsorbed on the weak Brønsted acid sites, while the high-temperature desorption peaks are attributed the NH_3 desorption adsorbed on the strong Lewis acid sites [29]. For the Mn-Ce-Ti(C) catalyst prepared by $MnC_4H_6O_4{\cdot}4H_2O$, it can generate relatively more Lewis acid sites, while the Mn-Ce-Ti(Cl) catalyst prepared by $MnCl_2{\cdot}4H_2O$ can yield more Brønsted acid sites. With

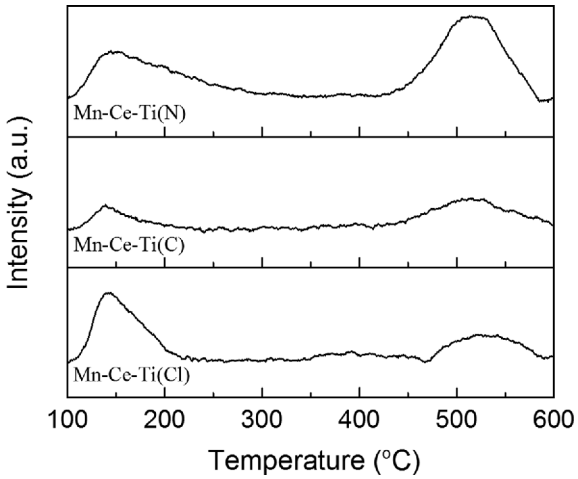

Fig. 5. NH_3-TPD profiles of different catalysts.

Table 3. NH_3-TPD results of different catalysts

Sample	Peak area (a.u.)		
	I	II	Total
Mn-Ce-Ti(N)	0.264	0.376	0.640
Mn-Ce-Ti(C)	0.067	0.176	0.243
Mn-Ce-Ti(Cl)	0.202	0.108	0.310

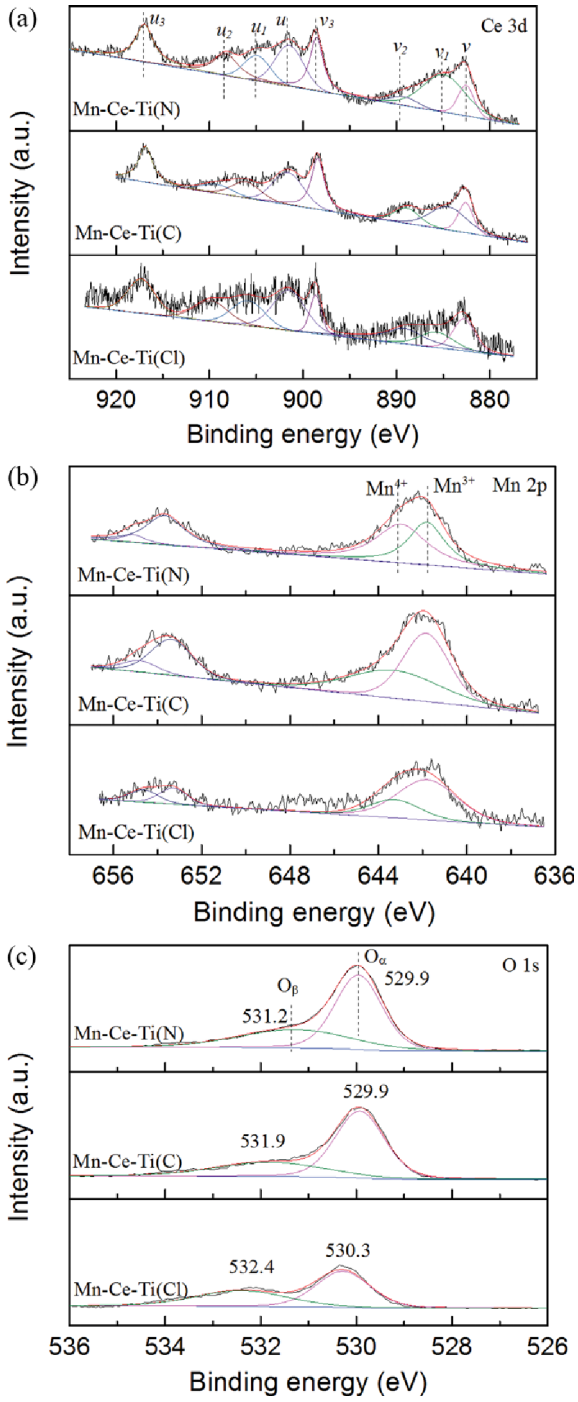

Fig. 6. XPS spectra of (a) Ce 3d, (b) Mn 2p, and (c) O 1s for the different catalysts.

Table 4. Atomic concentrations on the surface of the catalysts determined by XPS

Catalysts	Mn (%)	Ce (%)	Ti (%)	O (%)	Mn^{4+}/Mn^{3+}	$Ce^{3+}/(Ce^{3+}+Ce^{4+})$ (%)
Mn-Ce-Ti(N)	1.93	1.08	7.83	24.66	1.27	34.00
Mn-Ce-Ti(C)	1.92	1.03	6.55	22.32	0.81	27.21
Mn-Ce-Ti(Cl)	0.95	0.32	4.67	14.87	0.38	20.63

respect to the Mn-Ce-Ti(N) catalyst synthesized by $(Mn(NO_3)_2$, the amounts of Brønsted acid sites and the Lewis acid sites are both significantly enhanced. Therefore, more ammonia can be adsorbed on the Mn-Ce-Ti(N) catalyst surface in SCR reaction, which will lead to a superior catalytic activity of Mn-Ce-Ti(N) catalyst.

6. XPS Analysis

The XPS measurements were carried out to explore the surface element chemical states and surface atomic concentrations of different catalysts, and the results are displayed in Fig. 6 and Table 4. As shown in Fig. 6(a), the XPS spectra of Ce 3d for the three catalysts all can be divided into eight peaks labeled as v, v_1, v_2, v_3, u, u_1, u_2, and u_3, respectively. The peaks denoted as v_1 and u_1 are assigned to the surface Ce^{3+} species, while the peaks v, v_2, v_3, u, u_2, and u_3 are associated with the surface Ce^{4+} species [30,31]. This demonstrates that the Ce^{3+} and Ce^{4+} species coexist on the catalyst surface, which is beneficial for the creation of oxygen vacancies and charge imbalance, and thus results in a high concentration of surface chemisorbed oxygen [29]. As listed in Table 4, more Ce can be accumulated on the surface of the Mn-Ce-Ti(N) catalyst, and the ratio of $Ce^{3+}/(Ce^{3+}+Ce^{4+})$ over the three catalysts is determined to be 34.00, 27.21, and 20.63% for the Mn-Ce-Ti(N), Mn-Ce-Ti(C), Mn-Ce-Ti(Cl) catalyst, respectively. It fully demonstrates that the content of Ce^{3+} species is significantly affected by the Mn precursors of catalysts, and different Mn precursor will result in different interaction between Ce and Mn and thus generate a different concentration of Ce^{3+} species on the catalyst surface. The higher ratio of $Ce^{3+}/(Ce^{3+}+Ce^{4+})$ will facilitate the redox cycle of $Mn^{3+}+Ce^{4+}\leftrightarrow Mn^{4+}+Ce^{3+}$ and generate more oxygen vacancies, thus promoting the SCR performance of the catalyst. The Mn-Ce-Ti(N) catalyst holds the highest ratio of Ce^{3+} species and surface oxygen species, and therefore exhibits the best catalytic performance.

The Mn 2p spectra of the three catalysts are exhibited in Fig. 6(b). All the XPS spectra can be fitted into two peaks, which are attributed to the Mn^{4+} and Mn^{3+}, respectively [32,33]. The ratios of Mn^{4+}/Mn^{3+} for the three catalysts are calculated to be 1.27, 0.81, and 0.38 for the Mn-Ce-Ti(N), Mn-Ce-Ti(C), and Mn-Ce-Ti(Cl) catalyst, respectively, which is well consistent with the sequence of catalytic performance of the catalysts. This indicates that Mn precursor effect can lead to a different surface concentration of Mn^{4+} and Mn-Ce-Ti(N) possesses the highest ratio of Mn^{4+}/Mn^{3+}. It is well accepted that Mn^{4+} species play an important role in the SCR reaction. The higher ratio of Mn^{4+} will promote the conversion of NO to NO_2 and generate the "fast SCR" reaction, and thus accelerate the SCR performance [22,29,34]. Besides, the higher valence Mn oxide species are reported to be more active in the redox reaction so MnO_2 can yield superior catalytic activity compared to Mn_2O_3 [29,32,35]. The Mn-Ce-Ti(N) catalyst prepared by $(Mn(NO_3)_2$ precursor could form more dispersed MnO_x species on the catalyst surface and MnO_x species mainly exist as Mn^{4+}. Therefore, it can yield superior catalytic performance compared to the Mn-Ce-Ti(C) and Mn-Ce-Ti(Cl) catalyst.

Table 5. Binding energies of O1s and O_β concentration for different catalysts

Catalysts	Binding energies (eV)		O_β (%)
	O_α	O_β	
Mn-Ce-Ti(N)	529.9	531.2	9.2
Mn-Ce-Ti(C)	529.9	531.9	7.2
Mn-Ce-Ti(Cl)	530.3	532.4	6.3

Fig. 6(c) displays the O1s XPS spectra of the three catalysts. All of the spectra can be fitted into two peaks, which are assigned to the lattice oxygen (labeled as O_α) and surface chemisorbed oxygen (denoted as O_β), respectively [27,36-38]. The concentration of O for the Mn-Ce-Ti(N), Mn-Ce-Ti(C), and Mn-Ce-Ti(Cl) catalyst is obtained to be 9.2, 7.2, and 6.3%, respectively. It suggests that Mn precursor effect could generate a different concentration of O_β on the catalyst surface. It is well known that the surface chemisorbed oxygen possesses higher oxygen mobility than the lattice oxygen and can facilitate the oxidation of NO to NO_2, which can generate "fast SCR" reaction and therefore promote the SCR catalytic performance [2,11,39,40]. Besides, as listed in Table 5, the binding energies of O_α and O_β over Mn-Ce-Ti(N) catalyst are 529.9 and 531.2 eV, respectively. They are obviously lower than that of Mn-Ce-Ti(C) and Mn-Ce-Ti(Cl) catalyst. A lower BE value implies an element on the catalyst surface is more active and the catalyst can exhibit better catalytic performance. It is to say the surface chemisorbed oxygen and lattice oxygen over Mn-Ce-Ti(N) catalyst hold the most electron cloud density and thus can promote the formation of the reactive electrophilic oxygen species, and therefore will yield superior catalytic activity [27,41,42].

7. TEM and HR-TEM Analysis

TEM and HR-TEM were conducted to explore the morphology and crystal planes of catalysts prepared by different Mn precursors, and the results are exhibited in Fig. 7. It can be clearly seen that the particle sizes, dispersion and crystal planes of catalysts synthesized by different Mn precursors are significantly different. As shown in Fig. 7(a)-(c), the Mn-Ce-Ti(N) catalyst exhibits a high dispersion of active species on the catalyst support and holds the uniform distribution of particle sizes in the range of 4-15 nm. For the Mn-Ce-Ti(C) catalyst, it displays relatively poor dispersion of active species on the support and active species agglomerate to a certain extent on the local surface of the catalyst as marked with red dotted circles in Fig. 7(e)-(g). The particle sizes are mainly in the range of 6-30 nm, which exhibits relatively poor particle sizes distribution. With respect to the Mn-Ce-Ti(Cl) catalyst, it produces the poorest dispersion of active species on the catalyst surface.

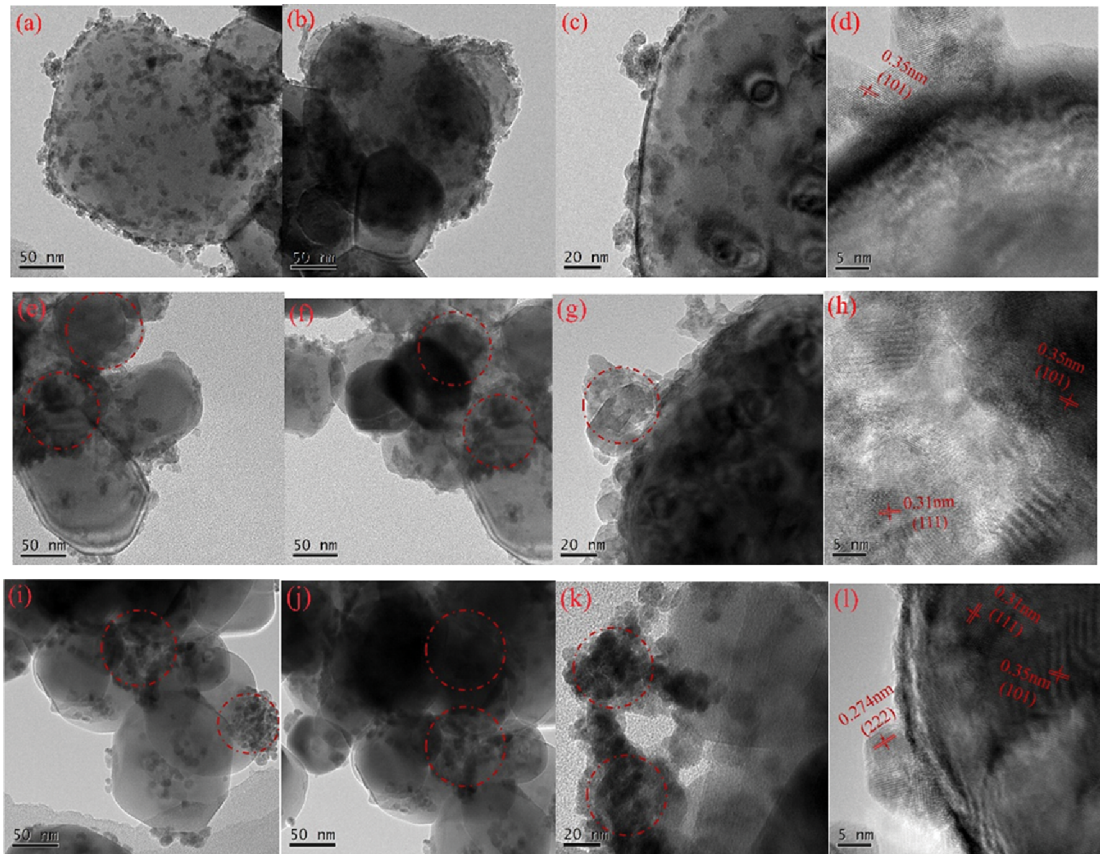

Fig. 7. TEM and HR-TEM images of different catalysts. (a)-(d) Mn-Ce-Ti(N), (e)-(h) Mn-Ce-Ti(C), and (i)-(l) Mn-Ce-Ti(Cl).

Some active species are severely agglomerated in the local area and are not highly precipitated and dispersed on the catalyst support as shown in the marked area in Fig. 7(k). Moreover, the precursor effect greatly influenced the crystal-plane characteristics of catalysts. All the three catalysts exhibit the same lattice fringes with the lattice spacing of 0.35nm, which is ascribed to the (101) plane of anatase TiO_2 planes [40,43,44]. The determined lattice spacing of 0.31 nm detected in Mn-Ce-Ti(C) and Mn-Ce-Ti(Cl) catalyst is attributed to the (111) plane of CeO_2 [45,46], while the obtained lattice spacing of 0.274 nm only observed in Mn-Ce-Ti(Cl) catalyst is assigned to the (222) plane of Mn_2O_3 [47-49]. These results demonstrate that the catalysts prepared by different Mn precursors could generate different crystal-plane features. For the Mn-Ce-Ti(N) catalyst prepared by $(Mn(NO_3)_2$ precursor, no visible lattice fringes corresponding to MnO_x and CeO_2 are detected except the anatase TiO_2 planes. While the same phenomenon is not observed on the Mn-Ce-Ti(C) and Mn-Ce-Ti(Cl) catalyst. Therefore, we may assume that the active species exist as an amorphous phase and are highly dispersed on Mn-Ce-Ti(N) catalyst surface, while a certain degree of crystallization may occur on the Mn-Ce-Ti(C) and Mn-Ce-Ti(Cl) catalyst surface.

Based on the results of different characterization analysis discussed above, the precursor effect could generate different dispersion and particle sizes of active species, and lead to different physicochemical properties of catalysts. The Mn-Ce-Ti(N) catalyst synthesized by $(Mn(NO_3)_2$ precursor yields the best dispersion and relatively more uniformity particle sizes of active species among the three catalysts. The higher dispersion and smaller particle sizes will inhibit the crystallinity of active species and enlarge the specific surface area, and thus promote the accumulation of active species on the catalyst surface. The enhanced accumulation of surface active species will provide more active sites in the SCR reaction and therefore exhibit superior catalytic performance. These may be the main reasons for the excellent catalytic activity of Mn-Ce-Ti(N) catalyst.

8. SEM-EDS Mapping Analysis

The SEM-EDS mapping results of the studied catalysts present direct and solid evidence of the dispersion of the active species as shown in Fig. 8. For the Mn-Ce-Ti(N) catalyst displayed in Fig. 8(a), the Mn and Ce species are dispersed highly and evenly on the catalyst, and the distribution regions and characteristics of the Mn and Ce exhibit high consistency, which suggests an interplay between Mn and Ce. With respect to the Mn-Ce-Ti(C) and Mn-Ce-Ti(Cl) catalysts, the dispersion of Mn and Ce is uneven and some obvious agglomeration of Mn over the two catalysts could be detected; the distribution regions of the Mn and Ce over the Mn-Ce-Ti(Cl) catalyst show significant differences. These results clearly illustrate that the precursor effect could greatly influence the dispersion of active species on the catalyst surface and Mn-Ce-Ti(N) catalyst prepared by manganese nitrate holds the best dispersion of active species (Mn and Ce), and therefore could yield the best catalytic activity.

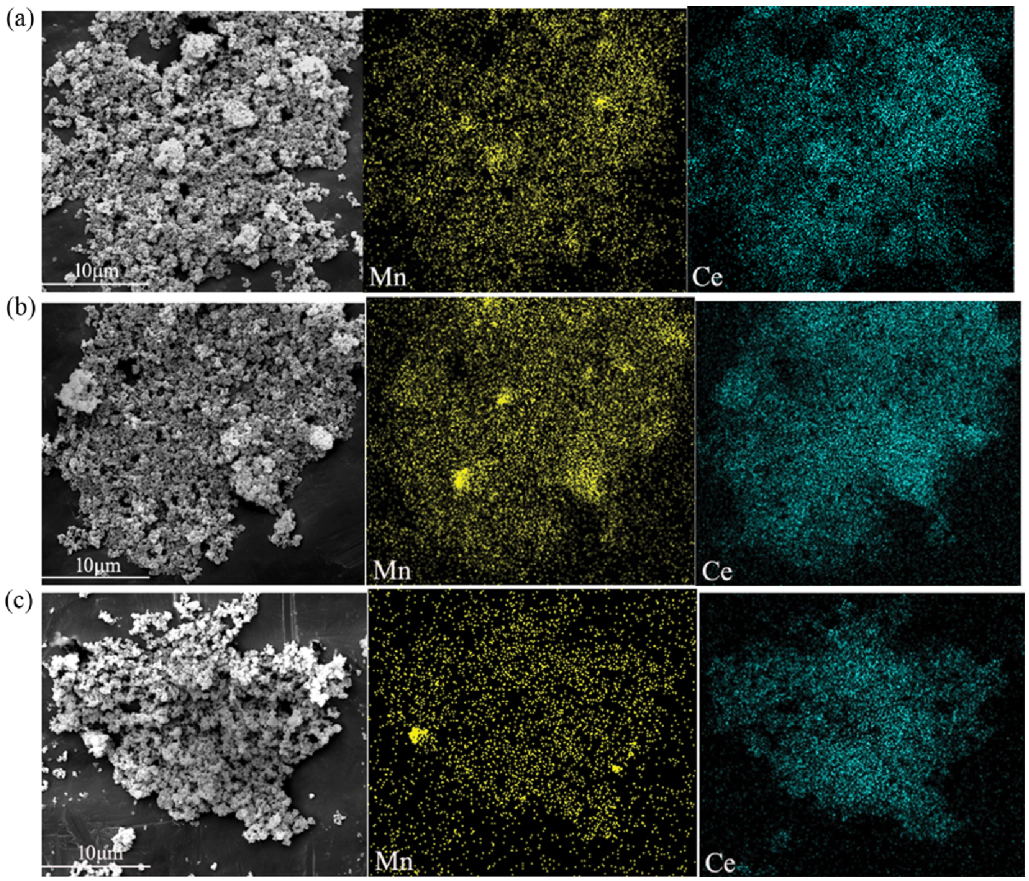

Fig. 8. Energy dispersive spectroscopy (EDS) mapping of different catalysts. (a) Mn-Ce-Ti(N), (b) Mn-Ce-Ti(C), and (c) Mn-Ce-Ti(Cl).

CONCLUSIONS

Mn-Ce-Ti catalysts were prepared by different precursors and used for NO abatement. The relationships among the structure, physicochemical properties, and catalytic activity were explored by various characterization methods. The results show that the different Mn precursors play important roles in the catalytic activity, and Mn-Ce-Ti(N) catalyst synthesized by $(Mn(NO_3)_2$ precursor exhibits the best catalytic activity. The superior catalytic performance may be ascribed to the high dispersion and uniformity of active species, the enhanced specific surface area, the promoted redox ability, the advanced surface acidity, the increased amounts of surface active species such as Mn^{4+}, Ce^{3+} and surface chemisorbed oxygen.

ACKNOWLEDGEMENTS

This work was supported by the National Natural Science Foundation of China (51276039), the Natural Science Foundation of the Jiangsu Higher Education Institutions of China (17KJB610005), the Jiangsu Government Scholarship for Overseas Studies (JS-2018), and a project funded by Nanjing Xiaozhuang University (2016NXY41).

SUPPORTING INFORMATION

Additional information as noted in the text. This information is available via the Internet at http://www.springer.com/chemistry/journal/11814.

REFERENCES

1. S. Campisi, M. G. Galloni, F. Bossola and A. Gervasini, *Catal. Commun.*, **123**, 79 (2019).
2. X. Zhang, J. Wang, Z. Song, H. Zhao, Y. Xing, M. Zhao, J. Zhao, Z. A. Ma, P. Zhang and N. Tsubaki, *Mol. Catal.*, **463**, 1 (2019).
3. R. T. Guo, X. Sun, J. Liu, W. G. Pan, M. Y. Li, S. M. Liu, P. Sun and S. W. Liu, *Appl. Catal. A*, **558**, 1 (2018).
4. P. Sun, S. X. Huang, R. t. Guo, M. Y. Li, S. M. Liu, W. G. Pan, Z. G. Fu, S. W. Liu, X. Sun and J. Liu, *Appl. Surf. Sci.*, **447**, 479 (2018).
5. Y. Ma, D. Zhang, H. Sun, J. Wu, P. Liang and H. Zhang, *Ind. Eng. Chem. Res.*, **57**, 3187 (2018).
6. J. Liu, R. T. Guo, M. Y. Li, P. Sun, S. M. Liu, W. G. Pan, S. W. Liu and X. Sun, *Fuel*, **223**, 385 (2018).
7. C. Chen, W. Jia, S. Liu and Y. Cao, *J. Mater. Sci.*, **53**, 10001 (2018).
8. T. Wang, H. Liu, X. Zhang, Y. Guo, Y. Zhang, Y. Wang and B. Sun, *Fuel Process. Technol.*, **158**, 199 (2017).
9. S. Han, Q. Ye, S. Cheng, T. Kang and H. Dai, *Catal. Sci. Technol.*, **7**, 703 (2017).
10. L. J. France, Q. Yang, W. Li, Z. Chen, J. Guang, D. Guo, L. Wang and X. Li, *Appl. Catal. B*, **206**, 203 (2017).
11. T. Boningari, P. R. Ettireddy, A. Somogyvari, Y. Liu, A. Vorontsov,

C. A. McDonald and P. G. Smirniotis, *J. Catal.*, **325**, 145 (2015).
12. G. Qi and R. T. Yang, *J. Catal.*, **217**, 434 (2003).
13. G. Carja, Y. Kameshima, K. Okada and C. D. Madhusoodana, *Appl. Catal. B*, **73**, 60 (2007).
14. G. Qi, R. T. Yang and R. Chang, *Catal. Lett.*, **87**(1-2), 67 (2003).
15. D. Fang, J. Xie, H. Hu, H. Yang, F. He and Z. Fu, *Chem. Eng. J.*, **271**, 23 (2015).
16. S. Hwang, S. H. Jo, J. Kim, M. C. Shin, H. H. Chun, H. Park and H. Lee, *React. Kinet. Mech Catal.*, **117**, 583 (2015).
17. D. A. Peña, B. S. Uphade and P. G. Smirniotis, *J. Catal.*, **221**, 421 (2004).
18. W. Xu, G. Zhang, H. Chen, G. Zhang, Y. Han, Y. Chang and P. Gong, *Chin. J. Catal.*, **39**, 118 (2018).
19. M. Lykaki, E. Pachatouridou, E. Iliopoulou, S. A. C. Carabineiro and M. Konsolakis, *RSC Adv.*, **7**, 6160 (2017).
20. X. Chen, S. A. C. Carabineiro, S. S. T. Bastos, P. B. Tavares, J. J. M. Órfão, M. F. R. Pereira and J. L. Figueiredo, *Appl. Catal. A*, **472**, 101 (2014).
21. S. A. C. Carabineiro, S. S. T. Bastos, J. J. M. Órfão, M. F. R. Pereira, J. J. Delgado and J. L. Figueiredo, *Catal. Lett.*, **134**, 217(2009).
22. Q. Li, X. Li, W. Li, L. Zhong, C. Zhang, Q. Fang and G. Chen, *Chem. Eng. J.*, **369**, 26 (2019).
23. D. W. Kwon, K. B. Nam and S. C. Hong, *Appl. Catal. A*, **497**, 160 (2015).
24. L. Xu, C. Wang, H. Chang, Q. Wu, T. Zhang and J. Li, *Environ. Sci. Technol.*, **52**, 7064 (2018).
25. J. Li, Y. Peng, H. Chang, X. Li, J. C. Crittenden and J. Hao, *Front. Environ. Sci. Eng.*, **10**, 413 (2016).
26. H. Chen, Y. Xia, H. Huang, Y. Gan, X. Tao, C. Liang, J. Luo, R. Fang, J. Zhang, W. Zhang and X. Liu, *Chem. Eng. J.*, **330**, 1195 (2017).
27. Z. Song, Q. Zhang, P. Ning, J. Fan, Y. Duan, X. Liu and Z. Huang, *J. Taiwan Inst. Chem. Eng.*, **65**, 149 (2016).
28. Q. Xu, R. Su, L. Cao, Y. Li, C. Yang, Y. Luo, J. Street, P. Jiao and L. Cai, *RSC Adv.*, **7**, 48785 (2017).
29. L. Jiang, Q. Liu, G. Ran, M. Kong, S. Ren, J. Yang and J. Li, *Chem. Eng. J.*, **370**, 810 (2019).
30. N. Wang, W. Qian, W. Chu and F. Wei, *Catal. Sci. Technol.*, **6**, 3594 (2016).
31. S. Zhan, H. Zhang, Y. Zhang, Q. Shi, Y. Li and X. Li, *Appl. Catal. B.*, **203**, 199 (2017).
32. X. Wang, X. Li, Q. Zhao, W. Sun, M. Tade and S. Liu, *Chem. Eng. J.*, **288**, 216 (2016).
33. W. Mu, J. Zhu, S. Zhang, Y. Guo, L. Su, X. Li and Z. Li, *Catal. Sci. Technol.*, **6**, 7532 (2016).
34. Y. J. Kim, H. J. Kwon, I. Heo, I. S. Nam, B. K. Cho, J. W. Choung, M. S. Cha and G. K. Yeo, *Appl. Catal. B*, **126**, 9 (2012).
35. J. Huang, H. Huang, L. Liu and H. Jiang, *Mol. Catal.*, **446**, 49 (2018).
36. Y. Shu, H. Sun, X. Quan and S. Chen, *J. Phys. Chem. C*, **116**, 25319 (2012).
37. L. Zhu, Y. Zeng, S. Zhang, J. Deng and Q. Zhong, *J. Environ. Sci. (China)*, **54**, 277 (2017).
38. Z. Qu, L. Miao, H. Wang and Q. Fu, *Chem. Commun. (Camb)*, **51**, 956 (2015).
39. L. Zhang, D. Zhang, J. Zhang, S. Cai, C. Fang, L. Huang, H. Li, R. Gao and L. Shi, *Nanoscale*, **5**, 9821 (2013).
40. W. Zhao, Q. Zhong, Y. Pan and R. Zhang, *Chem. Eng. J.*, **228**, 815 (2013).
41. X. Wang, S. Wu, W. Zou, S. Yu, K. Gui and L. Dong, *Chin. J. Catal.*, **37**, 1314 (2016).
42. B. Shen, H. Ma, C. He and X. Zhang, *Fuel Process. Technol.*, **119**, 121 (2014).
43. H. Wang, S. Cao, Z. Fang, F. Yu, Y. Liu, X. Weng and Z. Wu, *Appl. Surf. Sci.*, **330**, 245 (2015).
44. P. Zhang, C. Shao, X. Li, M. Zhang, X. Zhang, Y. Sun and Y. Liu, *J. Hazard. Mater.*, **237-238**, 331 (2012).
45. Y. Zhang, W. Guo, L. Wang, M. Song, L. Yang, K. Shen, H. Xu and C. Zhou, *Chin. J. Catal.*, **36**, 1701 (2015).
46. W. Yao, Y. Liu and Z. Wu, *Appl. Surf. Sci.*, **442**, 156 (2018).
47. X. You, Z. Sheng, D. Yu, L. Yang, X. Xiao and S. Wang, *Appl. Surf. Sci.*, **423**, 845 (2017).
48. Y. Shao, B. Ren, H. Jiang, B. Zhou, L. Lv, J. Ren, L. Dong, J. Li and Z. Liu, *J. Hazard. Mater.*, **333**, 222 (2017).
49. L. Lan, Q. Li, G. Gu, H. Zhang and B. Liu, *J. Alloy Compd.*, **644**, 430 (2015).